Earthquakes and Structures, Vol. 1, No. 4 (2010) 371-390
DOI: http://dx.doi.org/10.12989/eas.2010.1.4.371

Earthquake-induced pounding between the main buildings of the "Quinto Orazio Flacco" school

Alessandra Fiore* and Pietro Monaco

Politecnico di Bari, Department of Civil and Environmental Engineering, Via Orabona 4, 70125 Bari, Italy

(Received April 22, 2010, Accepted September 7, 2010)

Abstract. Historical buildings in seismically active regions are severely damaged by earthquakes, since they certainly were not designed by the original builders to withstand seismic effects. In particular the reports after major ground motions indicate that earthquake-induced pounding between buildings may lead to substantial damage or even collapse of colliding structures. The research on structural pounding during earthquakes has been recently much advanced, although most of the studies are conducted on simplified single degree of freedom systems. In this paper a detailed pounding-involved response analysis of three adjacent structures is performed, concerning the main bodies of the "Quinto Orazio Flacco" school. The construction includes a main masonry building, with an M-shaped plan, and a reinforced concrete building, separated from the masonry one and realized along its free perimeter. By the analysis of the capacity curves obtained by suitable pushover procedures performed separately for each building, it emerges that masonry and reinforced concrete buildings are vulnerable to earthquake-induced structural pounding in the longitudinal direction. In particular, due to the geometric configuration of the school, a special case of impact between the reinforced concrete structure and two parts of the masonry building occurs. In order to evaluate the pounding-involved response of three adjacent structures, in this paper a numerical procedure is proposed, programmed using MATLAB software. Both a non-linear viscoelastic model to simulate impact and an elastic-perfectly plastic approximation of the storey shear force-drift relation are assumed, differently from many commercial softwares which admit just one non-linearity.

Keywords: pushover analysis; earthquake-induced pounding; colliding structures; masonry building; reinforced concrete building; non-linear behaviour.

1. Introduction

The construction of the main masonry building of the "Quinto Orazio Flacco" school goes back to the year 1933, when the school became a point of reference for the educational training of young people not only of the city of Bari but of the entire Province (Fig. 1). The three-storey masonry building is characterized by an M-shaped plan with maximum dimensions equal to 57.8 m and 82.4 m, respectively in the transversal and longitudinal directions. The typologies of masonry employed are of three kinds: irregular quarrystones, carried out with stones crumbled up by hammer and overlapped on alternate courses (placed is situ) in order to avoid the recurrence of the vertical joints between consecutive returns; claved stone blocks worked by marteline, broken into regular pieces with sharp corners on the external face and joined together with 3 mm thick mortar; tufa

* Corresponding author, Ph.D., E-mail: a.fiore@poliba.it

parallelepiped-shaped blocks, in different sizes ranging from 32 to 90 cm, with perfectly squared faces and sharp corners, joined together with 1 cm thick cement mortar. The documents available and the tests carried out with some single masonry units have shown that foundation walls are in

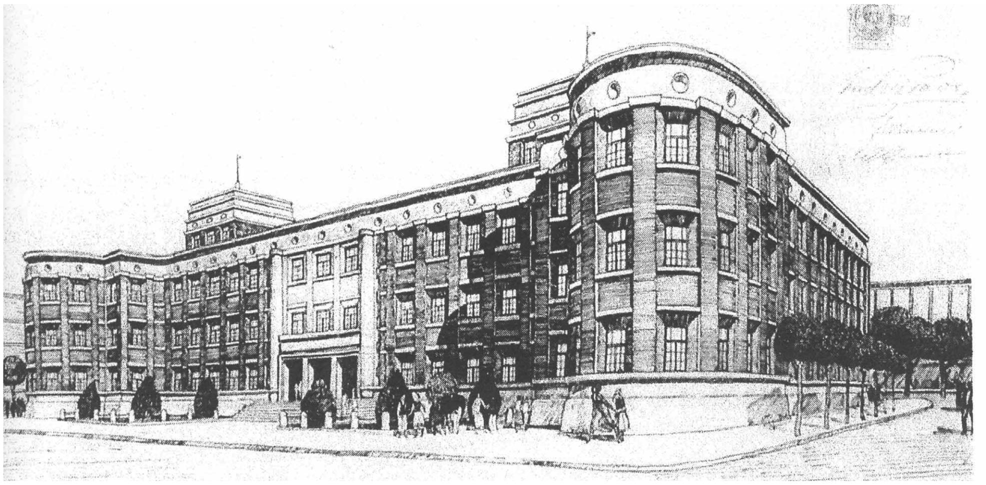

Fig. 1 Perspective view of the “Quinto Orazio Flacco” school, 1933

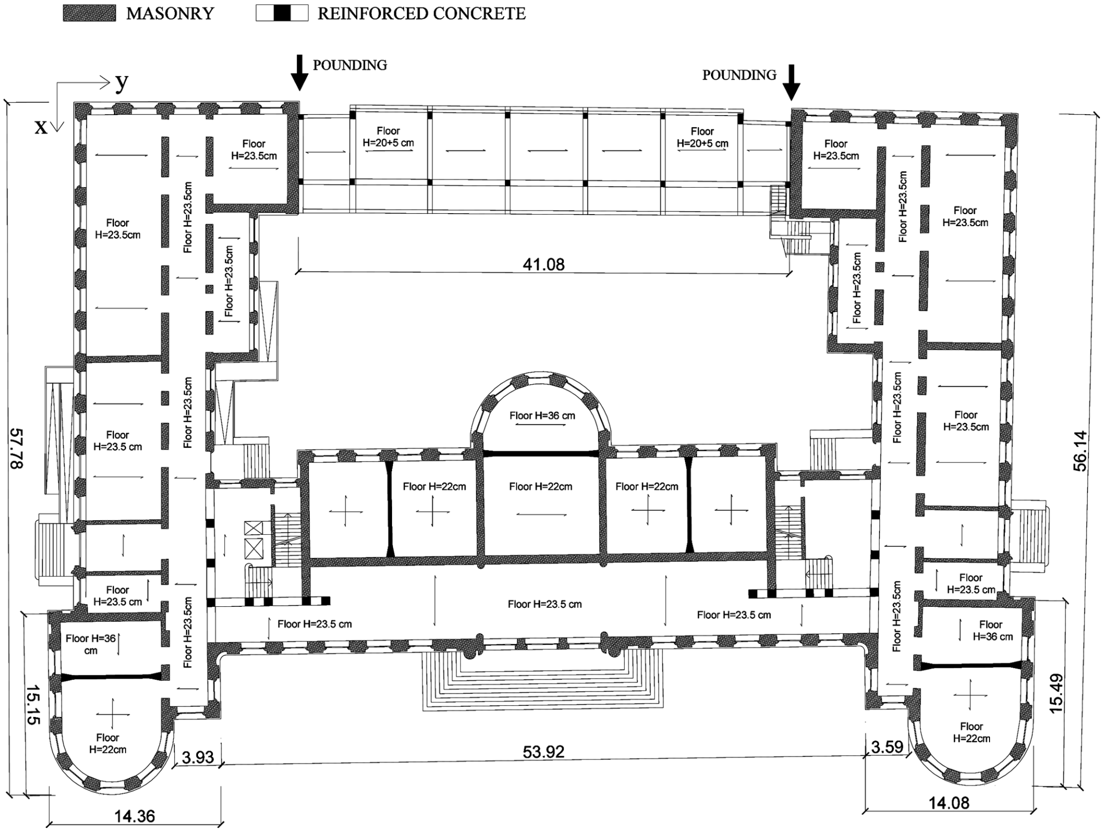

Fig. 2 Ground floor of masonry and reinforced concrete buildings

irregular quarrystones and basement walls are in claved stone blocks. Contrarily ground floor walls are in different materials: internal walls are in tufa blocks, while external ones are in claved stone blocks covered by "mazzaro" tufa units. Finally on the upper floors claved stone blocks have been replaced by tufa blocks. The staircase spaces, the architraves for wide openings and the horizontal structures are realized in reinforced concrete. In particular floors consist of reinforced concrete beams with an infill between them made of hollow clay blocks and have a total height varying according to the span ($H = 22$, 23.5, 36 cm).

In 1963, dictated by the necessity of finding further premises, a new reinforced concrete building, separated from the pre-existent masonry one, was realized along its free perimeter. Fig. 2 shows the ground floor of the final buildings. The separation gaps between masonry and concrete buildings are about 2 cm.

Moreover, in the long run, other variants were realized above all in the ground floor of the masonry building, damaging the functionality and aesthetics of this floor. In particular smaller school-rooms have been obtained by dividing the bigger ones with partition walls; these often divide into two the windows, too.

The partition walls, probably leaning directly on the floor, have suffered evident cracks which have more than once been repaired. Of course the presence of new rooms has made it necessary to realize new openings on the longitudinal walls, reducing their resistance.

In the light of the complexity of the described case study, it emerges the necessity to asses the seismic safety of both masonry and reinforced concrete buildings and to investigate the level of seismic pounding risk of the adjacent structures.

2. Pushover analysis

Static incremental analyses allow us to define the seismic capacity of structures. Pushover analysis is a non-linear static procedure carried out under conditions of constant gravity loads and increasing horizontal loads (CEN 2003, M.I.T 2008). In particular the values of the latter are increased monotonically step by step, until a failure mechanism is achieved. Herein two different lateral load distributions are used: a "uniform" pattern, with a force applied at each node proportional to the mass tributary to that node; a "modal" pattern, with a force applied at each node proportional to the product of the displacement of the node in the first mode shape times the mass (tributary to that node). In fact, referring to both masonry and reinforced concrete buildings, the effective modal mass of each fundamental mode in longitudinal and transversal directions amounts to at least 58% of the total mass of the structure. A vertical load equal to $G_k + 0.6Q_k$ is introduced at step 0 and then kept unchanged in the process of pushover. Since both masonry and reinforced concrete buildings must be analysed for each pattern of lateral forces and for both transversal and longitudinal directions, eight pushover analyses are totally performed. Each analysis leads to the capacity curve, i.e. the base shear force versus the displacement of the control point (middle point at the top of the building). After each pushover curve of the actual multi-degree-of-freedom (MDOF) structure is plotted, it must be scaled by the transformation factor Γ (CEN 2003), in order to use its bilinear approximation to define the yield force and displacement of the equivalent single-degree-of-freedom (SDOF) system. The former values allow us to determine the elastic period T^* of the idealised elastic-perfectly plastic SDOF model; the displacement demand (target displacement) of the structure with period T^* associated to the seismic performance level under consideration can be estimated through the elastic response spectrum at the period T^*. Finally the seismic performance of the structure is assessed for the required hazard intensity transforming back the displacement demand from the SDOF system to the MDOF one.

2.1 Finite element model

Masonry is treated as a non-linear homogeneous orthotropic material consisting of units and mortar. In order to correctly simulate the behaviour of the masonry building, since sufficient anchorage and bond of masonry units is provided, an equivalent frame element model is used, characterized by an assemblage of pier, spandrel and joint panels (Salonikios *et al.* 2003, Mistler *et al.* 2006). Pier and spandrel panels represent, respectively, masonry vertical and horizontal bearing elements, while joint panels are rigid elements linking pier and spandrel panels together. The dimensions of pier, spandrel and joint panels, expected to sustain gravity and lateral loads, are defined by the geometric arrangement of the openings; more precisely the three types of macro-elements are derived by the intersection between the horizontal and vertical strips obtained by extending the contour lines of the openings. The horizontal floor diaphragms can be considered rigid in their own plane and adequately resistant to distribute lateral loads between piers, which can absorb in-plane forces; contrarily the pier resistance to out-of-plane loads is neglected. Also the tensile strength of masonry is neglected.

Piers and spandrels are modeled by assuming an elastic-perfectly plastic behaviour based on the plastic hinge concept. In fact it was found that unreinforced masonry buildings may exhibit ductile inelastic behaviour under combined vertical and horizontal loads: according to the Mohr-Coulumb criterion, in the high inelastic deformation range where cohesion ceases to exist, satisfactory ductility is provided by the friction (Magenes and Calvi 1997). Under this assumption, a necessary prerequisite is the definition of the possible locations and types of the plastic hinges that might develop along the span of each element. These plastic hinges should be able to accurately describe the possible failure mechanisms observed in the actual structures, subjected both to dead loads and seismic action. Depending on the width to height ratio of the element and on the respective values of normal force, bending moment and shear force, three failure mechanisms might occur: bending failure, shear failure and friction failure. In the present study a suitable moment-displacement (M-δ) plastic hinge is provided at both ends of each element (flexural mechanism), while a shear-displacement (V-δ) plastic hinge is located at the mid-span (shear mechanism).

With reference to pier panels, the flexural and shear resistances are expressed by (CEN 2005, P.C.M. 2005, Tomaževiĉ 1999)

$$M_u = \left(l^2 t' \frac{\sigma_o}{2}\right)\left(1 - \frac{\sigma_o}{0.85 f_d}\right); \; V_u = l' t f_{vd} \tag{1}$$

where: l and t' are the overall length and the compressed thickness of the panel, respectively; σ_o is the mean axial stress due to vertical loads; $f_d = f_k / \gamma_m$ is the design compressive strength of masonry; l' and t are the compressed length and the thickness of the panel, respectively; $f_{vd} = f_{vk} / \gamma_m$ is the design shear strength of masonry. The ultimate available displacements in the case of flexural ($\delta_{u,M}$) and shear ($\delta_{u,V}$) mechanisms are set, respectively, equal to 0.8%H and 0.4%H, H being the height of the panel. A reduced resistance, set according to FEMA (2000), is finally considered after the point of ultimate strength. The just described constitutive laws of piers are shown in Fig. 3(a).

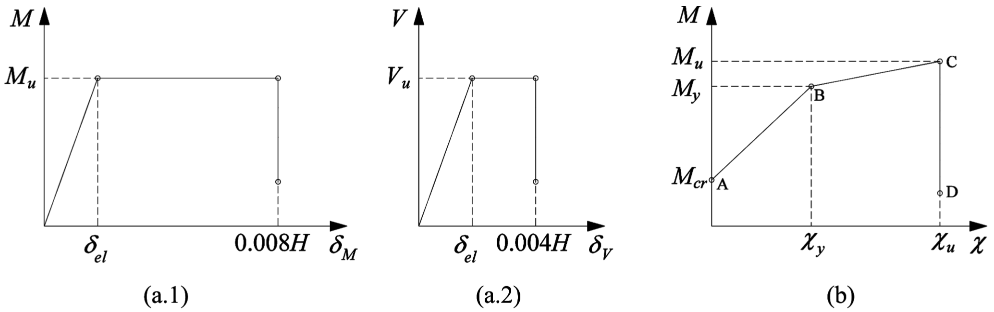

Fig. 3 Constitutive laws: (a) masonry panels, (b) concrete frame elements

Spandrel panels play a significant role in walls of existing unreinforced masonry buildings, as they guarantee an effective coupling between adjacent masonry piers and assure high in-plane strength and stiffness for the walls. The type of masonry structure studied in this paper is characterized by the presence, at each floor level in the proximity of spandrel beams, of internal reinforced-concrete ties capable of carrying tensile forces. Following this assumption, spandrel beams can be considered not just like purelly axially rigid elements but as flexural resistant panels. Nevertheless, differently from pier elements, under seismic loads masonry beams are subjected to shear and bending with negligible axial force. The flexural and shear resistances of spandrel beams in this case can be calculated by (P.C.M. 2005)

$$M_u = \frac{H_p h}{2[1 - H_p/(0.85 f_{hd} h t)]}; \; V_u = h t f_{vd0} \tag{2}$$

where: h and t are the height and the width of the beam section, respectively; H_p is the minimum value between the tensile strength of the horizontal panel in tension and the product $0.4 f_{hd} h t$, $f_{hd} = f_{hk}/\gamma_m$ being the design compressive strength of masonry in the horizontal direction; $f_{vd0} = f_{vk0}/\gamma_m$ is the design shear strength of masonry in absence of compression.

The reinforced concrete building is treated as a frame element model, in which the spread of inelasticity is implemented through the formation of non-linear plastic hinges at the frame element's ends during the incremental loading process. More precisely pure moments hinges and axial-moment hinges are assigned to the two ends of beams and columns, respectively.

The moment-rotation relationship of a plastic hinge is modelled as a trilinear curve (Fig. 3(b)): the elastic segment (AB), the hardening segment (BC) and the softening segment (CD), where point A corresponds to the cracking condition, point B is the first yield moment point and point C is the ultimate moment capacity.

Given the quantity of the steel reinforcement used in a concrete section, the values of the moments M_{cr}, M_y, M_u and of the curvatures χ_y, χ_u can be easily determined (CEN 2001, M.I.T 2008, Zou and Chan 2005).

2.2 Analysis results

The seismic acceleration spectrum adopted in the present paper is calculated according to Italian code (M.I.T 2008). The following design conditions are adopted:

- nominal expected life of the structure: $V_n = 50$ years;
- utilization coefficient of the structure: 4^{th} Class ($C_u = 2$);

- reference period for the seismic action: $V_R = V_n\ C_u = 100$ years.

Seismic zone is identified by the following characteristics:
- longitude: 16.51°;
- latitude: 41.07°;
- ground type: A (soil factor $S = 1$).

Seismic hazard parameters of the site are given by:
- design ground acceleration for the no-collapse requirement (NCR): $a_g = 0.281$ g;
- maximum amplification factor of the acceleration response spectrum: $F_o = 2.368$;
- upper period of the constant acceleration branch of the response spectrum: $T_C^* = 0.394$.

The upper acceleration value of the constant branch of the design response spectrum is then equal to 0.44 g.

The values of the mechanical properties of materials, used for numerical simulation, are based on laboratory tests and are reported in Tables 1 and 2, where ρ_i, E_i and ν_i ($i = m$, c) represent the unit weight, the Young's modulus and the Poisson's ratio of masonry ($i = m$) and concrete ($i = c$), respectively, while E_s is the Young's modulus of reinforcement. Moreover in Table 2 f_{cd} and $f_{cfm,d}$ are the design compressive strength and mean tensile strength of concrete, respectively, while f_{yd} is the design yield strength of steel.

Non-linear static analyses of both masonry and reinforced concrete buildings are performed by using detailed three-dimensional finite elements models of the two structures; in particular finite elements codes MIDAS Gen and SAP2000 are used, respectively.

Table 1. Masonry properties

Masonry type	ρ_m [kN/m^3]	E_m [kN/m^2]	ν_m	f_d [kN/m^2]	f_{vd} [kN/m^2]	f_{hd} [kN/m^2]	f_{vdo} [kN/m^2]
Tufa blocks	18	$2{\cdot}10^6$	0.25	1400	28	700	25
Claved stone blocks	22	$3.4{\cdot}10^6$	0.25	6000	90	3000	84

Table 2. Reinforced concrete properties

ρ_c [kN/m^3]	E_c [kN/m^2]	ν_c	f_{cd} [kN/m^2]	$f_{cfm,d}$ [kN/m^2]	E_s [kN/m^2]	f_{yd} [kN/m^2]
25	$3.14{\cdot}10^7$	0.2	12000	2260	$2.06{\cdot}10^8$	300000

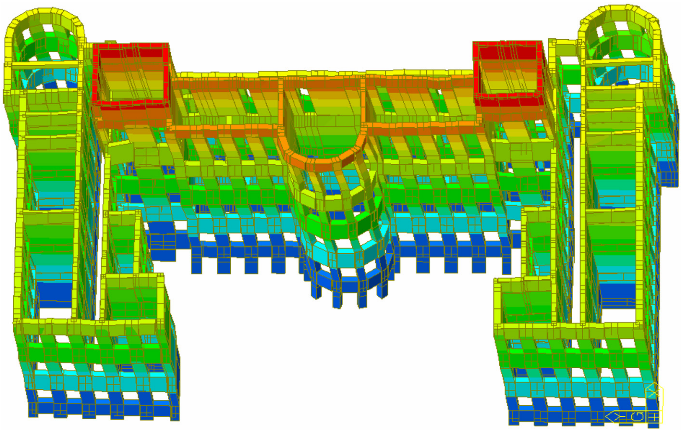

Fig. 4 1st mode of vibration of the masonry building: $T = 0.27$ s, $M_{x\%} = 1.37\%$, $M_{y\%} = 58.36\%$

Figs. 4 and 5 show the first and second modes of vibration of the masonry building: the first one is the fundamental mode in the longitudinal (y) direction, with period $T = 0.27$ s, while the second is the fundamental mode in the transversal (x) direction with period $T = 0.26$ s.

The capacity curves obtained by the pushover analyses performed for each direction and for both uniform and modal patterns are reported in Fig. 6. Fig. 6 also shows the final target displacements of the MDOF system associated to the Collapse Prevention (CP) seismic performance level. Observing the results obtained, it emerges that the deformation capacity of the masonry building is superior than the demand associated to the CP performance state.

Figs. 7(a) and (b) show the first and second modes of vibration of the reinforced concrete building: the first one is the fundamental mode in the longitudinal (y) direction, with period $T = 1.48$ s, while the second is the fundamental mode in the transversal (x) direction with period $T = 0.98$ s. The capacity curves obtained by the pushover analyses performed for each direction and for both uniform and modal patterns are reported in Fig. 8. The final target displacements of the MDOF

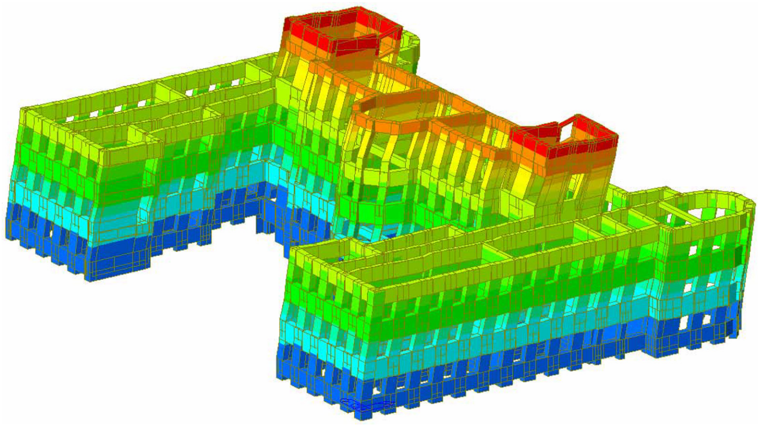

Fig. 5 2nd mode of vibration of the masonry building: $T = 0.26$ s, $M_{x\%} = 57.7\%$, $M_{y\%} = 1.3\%$

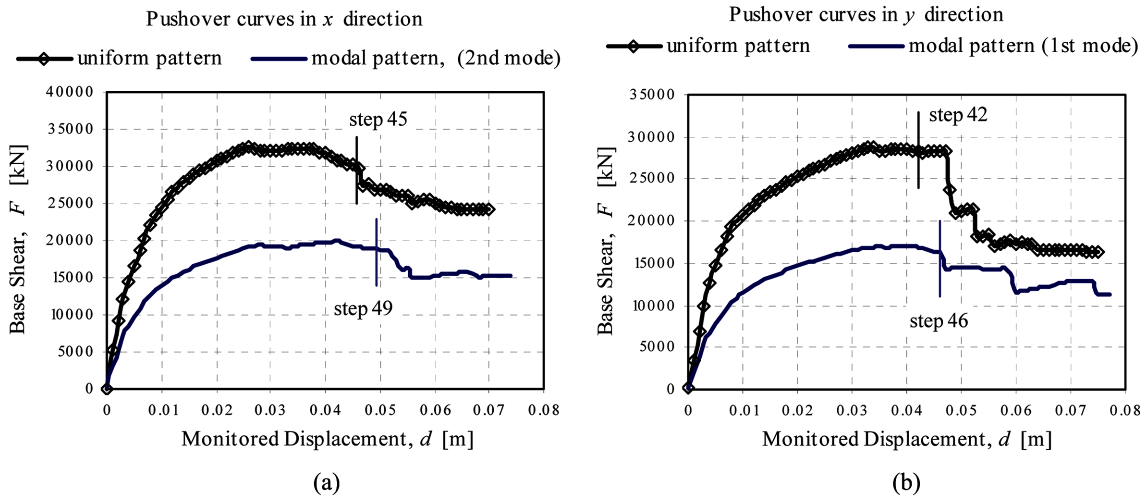

Fig. 6 Pushover curves and CP target displacements of the masonry building: (a) x direction, (b) y direction

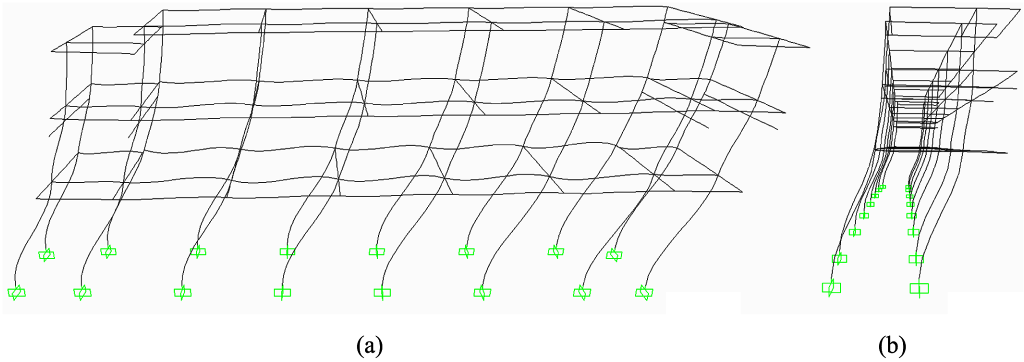

Fig. 7 Reinforced concrete building: (a) 1st mode of vibration: $T = 1.48$ s, $M_{x\%} = 0.0\%$, $M_{y\%} = 95.7\%$, (b) 2nd mode of vibration: $T = 0.98$ s, $M_{x\%} = 98.1\%$, $M_{y\%} = 0.0\%$

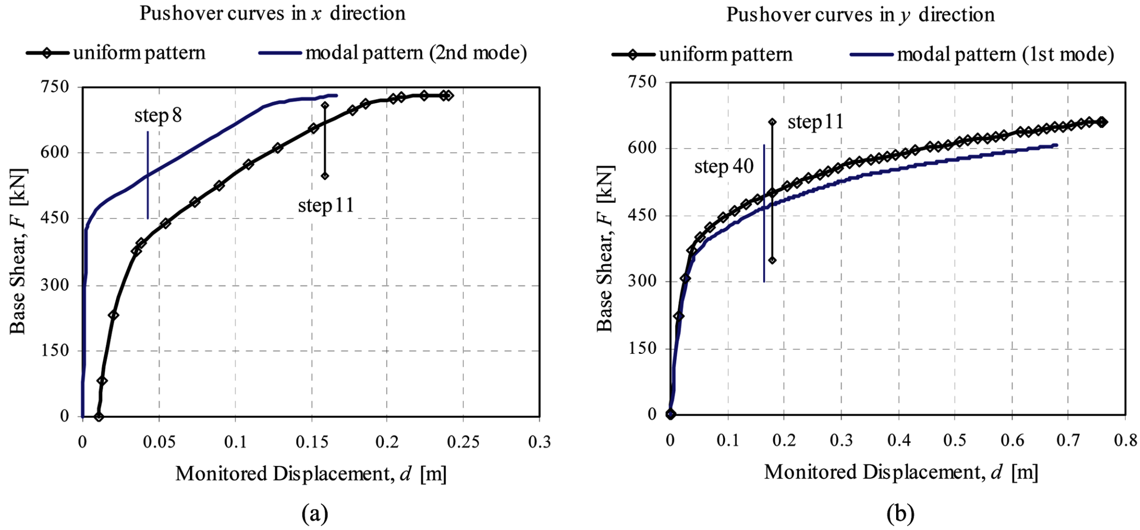

Fig. 8 Pushover curves and CP target displacements of the concrete building: (a) x direction, (b) y direction

system associated to the CP seismic performance level are also represented in Fig. 8.

The intersection between the capacity curve and the line associated to the target displacement defines the "performance point" of the structure. At the performance point, checking the capacity of the structure against the seismic demand in terms of sectional plastic rotations, it results that the reinforced concrete building has a good level of safety against seismic action.

3. Earthquake-induced structural pounding

Observing all the capacity curves obtained, that is the maximum allowable displacements of the control nodes, and taking into account that the separation gaps between masonry and reinforced concrete buildings are equal to 2 cm, it appears that the structures under examination are vulnerable to earthquake-induced structural pounding in the longitudinal direction. In particular, due to the geometric configuration of the school, a special case of impact between the reinforced concrete structure and two parts of the masonry building occurs. In fact the reinforced concrete building is situated between two bodies of the masonry one and building separations are insufficient to accommodate the relative motions of the three adjacent structures. In addition the adjacent buildings are characterized by natural vibration periods sensibly different, which produce out-of-phase vibrations. Therefore an earthquake-induced pounding simulation is performed, by means of non-linear time-history analyses.

3.1 Numerical procedure

The commercial Finite Element code MIDAS Gen allows us to perform pounding-involved response analyses simulating the impact by non-linear viscoelastic models, while just an elastic

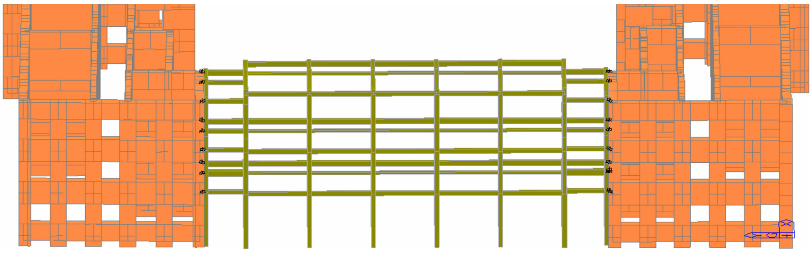

Fig. 9 MIDAS Gen model

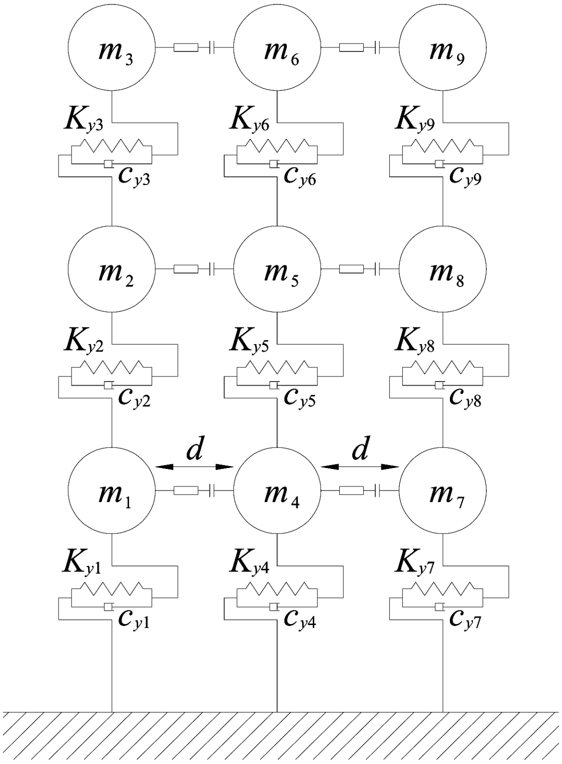

Fig. 10 Numerical model

behaviour of the storey shear force can be assumed. Nevertheless a time-history analysis of this type is preliminarily carried out since, referring to the three-dimensional model of the structures under examination described in § 2, it allows us to suitably calibrate some structural data to insert in the numerical algorithm herein proposed. Pounding between the three adjacent structures in the longitudinal direction is controlled by gap-friction elements placed between the nodes of the models at all the storey levels, as it is shown in Fig. 9.

As above mentioned, in order to evaluate more realistically the pounding-involved forces acting on the reinforced concrete and masonry buildings, a suitable numerical procedure is elaborated by MATLAB software. In this case, besides using a non-linear viscoelastic model to simulate impact, an elastic-perfectly plastic approximation of the storey shear force-drift relation is assumed. Each colliding 3-storey building is modelled like a three-degree-of-freedom system, with each storey's mass lumped on the floor level (Fig. 10). Torsional effects are neglected.

The dynamic equation of motion in the longitudinal direction for the described structural model can be written as

$$\boldsymbol{M}\cdot\ddot{\boldsymbol{y}}(t)+\boldsymbol{C}_y\cdot\dot{\boldsymbol{y}}(\boldsymbol{t})+\boldsymbol{F}_y^s(t)+\boldsymbol{F}_y(t) = -\boldsymbol{M}\cdot\ddot{\boldsymbol{y}}_g(t) \tag{3}$$

with

$$\ddot{\boldsymbol{y}}(t)=\begin{bmatrix}\ddot{y}_1(t)\\ \ddot{y}_2(t)\\ \ddot{y}_3(t)\\ \ddot{y}_4(t)\\ \ddot{y}_5(t)\\ \ddot{y}_6(t)\\ \ddot{y}_7(t)\\ \ddot{y}_8(t)\\ \ddot{y}_9(t)\end{bmatrix};\quad \dot{\boldsymbol{y}}(t)=\begin{bmatrix}\dot{y}_1(t)\\ \dot{y}_2(t)\\ \dot{y}_3(t)\\ \dot{y}_4(t)\\ \dot{y}_5(t)\\ \dot{y}_6(t)\\ \dot{y}_7(t)\\ \dot{y}_8(t)\\ \dot{y}_9(t)\end{bmatrix};\quad \boldsymbol{M}=\begin{bmatrix}m_1&0&0&0&0&0&0&0&0\\0&m_2&0&0&0&0&0&0&0\\0&0&m_3&0&0&0&0&0&0\\0&0&0&m_4&0&0&0&0&0\\0&0&0&0&m_5&0&0&0&0\\0&0&0&0&0&m_6&0&0&0\\0&0&0&0&0&0&m_7&0&0\\0&0&0&0&0&0&0&m_8&0\\0&0&0&0&0&0&0&0&m_9\end{bmatrix}$$

$$\boldsymbol{C}_y=\begin{bmatrix}c_{y1}+c_{y2}&-c_{y2}&0&0&0&0&0&0&0\\-c_{y2}&c_{y2}+c_{y3}&-c_{y3}&0&0&0&0&0&0\\0&-c_{y3}&c_{y3}&0&0&0&0&0&0\\0&0&0&c_{y4}+c_{y5}&-c_{y5}&0&0&0&0\\0&0&0&-c_{y5}&c_{y5}+c_{y6}&-c_{y6}&0&0&0\\0&0&0&0&-c_{y6}&c_{y6}&0&0&0\\0&0&0&0&0&0&c_{y7}+c_{y8}&-c_{y8}&0\\0&0&0&0&0&0&-c_{y8}&c_{y8}+c_{y9}&-c_{y9}\\0&0&0&0&0&0&0&-c_{y9}&c_{y9}\end{bmatrix}$$

$$\boldsymbol{F}_y^S(t) = \begin{bmatrix} F_{y1}^S(t) - F_{y2}^S(t) \\ F_{y2}^S(t) - F_{y3}^S(t) \\ F_{y3}^S(t) \\ F_{y4}^S(t) - F_{y5}^S(t) \\ F_{y5}^S(t) - F_{y6}^S(t) \\ F_{y6}^S(t) \\ F_{y7}^S(t) - F_{y8}^S(t) \\ F_{y8}^S(t) - F_{y9}^S(t) \\ F_{y9}^S(t) \end{bmatrix}; \quad \boldsymbol{F}_y(t) = \begin{bmatrix} F_{y14}(t) \\ F_{y25}(t) \\ F_{y36}(t) \\ -F_{y14}(t) + F_{y47}(t) \\ -F_{y25}(t) + F_{y58}(t) \\ -F_{y36}(t) + F_{y69}(t) \\ -F_{y47}(t) \\ -F_{y58}(t) \\ -F_{y69}(t) \end{bmatrix}; \quad \ddot{\boldsymbol{y}}_g(t) = \begin{bmatrix} \ddot{y}_g(t) \\ \ddot{y}_g(t) \\ \ddot{y}_g(t) \\ \ddot{y}_g(t) \\ \ddot{y}_g(t) \\ \ddot{y}_g(t) \\ \ddot{y}_g(t) \\ \ddot{y}_g(t) \\ \ddot{y}_g(t) \end{bmatrix}$$

where $\ddot{y}_i(t)$, $\dot{y}_i(t)$, $y_i(t)$ $(i = 1,\ldots,9)$ are the acceleration, velocity and displacement of a single storey in the longitudinal direction; $F_{yi}^S(t)$ $(i = 1,\ldots,9)$ are the inelastic storey shear forces; c_{yi} are the elastic damping coefficients; $F_{yij}(t)$ $(i = 1,\ldots,6)$ $(j = 4,\ldots,9)$ are the pounding forces between storeys with masses m_i, m_j; $\ddot{y}_g(t)$ is the longitudinal acceleration component of the input ground motion.

The storey shear forces, according to an elastic-perfectly plastic behaviour, are expressed for the elastic range by

$$F_{yi}^S(t) = K_{yi} y_i(t) \qquad (i = 1, 4, 7) \tag{4}$$

$$F_{yi}^S(t) = K_{yi}[y_i(t) - y_{i-1}(t)] \qquad (i = 2, 3, 5, 6, 8, 9) \tag{5}$$

and for the plastic range by

$$F_{yi}^S(t) = F_{yi}^Y \qquad (i = 1,\ldots,9) \tag{6}$$

K_{yi} and F_{yi}^Y $(i = 1,\ldots,9)$ being the elastic structural stiffness coefficients and the storey yield strengths, respectively. The pounding forces in the longitudinal direction are simulated according to the non-linear viscoelastic model based on the Hertz's contact law (Jankowski 2008)

$$F_{yij}(t) = 0 \quad \text{for} \quad \delta_{ij}(t) \le 0 \tag{7}$$

$$F_{yij}(t) = \beta \delta_{ij}^{\frac{3}{2}}(t) + \bar{c}_{ij}(t)\dot{\delta}_{ij}(t) \quad \text{for} \quad \delta_{ij}(t) > 0;\ \dot{\delta}_{ij}(t) > 0 \tag{8}$$

$$F_{yij}(t) = \beta \delta_{ij}^{\frac{3}{2}}(t) \quad \text{for} \quad \delta_{ij}(t) > 0;\ \dot{\delta}_{ij}(t) \le 0 \tag{9}$$

$$\delta_{ij}(t) = y_i(t) - y_j(t) - d \tag{10}$$

$$\bar{c}_{ij}(t) = 2\xi \sqrt{\beta \sqrt{\delta_{ij}(t)} \frac{m_i m_j}{m_i + m_j}} \tag{11}$$

where β is the impact stiffness parameter simulating the local stiffness at the contact point, d is the initial separation gap and ξ denotes the impact-damping ratio. The term ξ is estimated using Jankowski's formula (Jankowski 2006)

$$\xi = \frac{9\sqrt{5}}{2}\frac{1-e^2}{e[e(9\pi-16)+16]} \tag{12}$$

where e is the coefficient of restitution accounting for the energy dissipation during impact. The correct value of the coefficient e is obtained numerically through iterative simulations in order to satisfy the following relation between the post-impact (v_i') and the prior-impact (v_i) velocities (Jankowski 2005)

$$e = \frac{|v_i' - v_j'|}{v_i - v_j} \tag{13}$$

The impact stiffness parameter β depends on the material properties and geometry of colliding bodies and its value can be determined on the basis of experimental results; more precisely it can be obtained numerically through iterative simulations which tend to fit the experimentally obtained pounding force time histories. The formulae to calculate the value of β have been deduced only for certain impact cases, such as non-linear elastic contacts between two isotropic spheres (Jankowski 2005, Muthukumar and DesRoches 2006, Ye and Li 2009).

In order to solve the equation of motion (3) numerically, the initial value problem of the second order is transformed into a problem of the first order, by introducing the following system

$$\tilde{\boldsymbol{M}} \cdot \dot{\boldsymbol{Y}}(t) = \boldsymbol{A} \cdot \boldsymbol{Y}(t) + \tilde{\boldsymbol{F}}(t,y) \tag{14}$$

with

$$\boldsymbol{Y}(t) = \begin{bmatrix} \boldsymbol{y}(t) \\ \dot{\boldsymbol{y}}(t) \end{bmatrix}; \qquad \tilde{\boldsymbol{M}} = \begin{bmatrix} \boldsymbol{I}_{9x9} & \mathbf{0}_{9x9} \\ \mathbf{0}_{9x9} & \boldsymbol{M} \end{bmatrix}; \qquad \boldsymbol{A} = \begin{bmatrix} \mathbf{0}_{9x9} & \boldsymbol{I}_{9x9} \\ \mathbf{0}_{9x9} & -\boldsymbol{C}_y \end{bmatrix} \tag{15}$$

$$\tilde{\boldsymbol{F}}(t,y) = \begin{bmatrix} \mathbf{0}_9 \\ -\boldsymbol{F}_y(t) - \boldsymbol{F}_y^S(t) - \boldsymbol{M} \cdot \ddot{\boldsymbol{y}}_g(t) \end{bmatrix} \tag{16}$$

where $\boldsymbol{I}_{9x9}$ and $\mathbf{0}_{9x9}$ are 9x9 identity and zeros matrices, respectively, while $\mathbf{0}_9$ represents a 9-dimension column vector of zeros. The above transformation allows us to use suitable numerical solvers provided by MATLAB software, such as *ode15s*. The algorithm so obtained is structured in such a way to provide as output, for all possible values of structural parameters inserted in input, the displacements and pounding forces at contact points. The proposed procedure represents a simple and effective method for properly simulating the seismic-pounding response between three colliding structures; it allows us, with a small numerical burden, to take into account both impact and structural non-linearities, differently from many commercial softwares which admit just one non-linearity. This aspect makes the presented procedure particularly useful for practical purpose.

3.2 Analysis results

The accelerogram corresponding to the seismic motion considered in the present paper has been artificially generated using the design response spectrum described in § *2.2* (Fig. 11).

The basic values describing the structural characteristics of the buildings under examination have been obtained by the FE three-dimensional model and are herein summarized

$m_1 = m_7 = 2814264$ kg, $m_2 = m_8 = 1708400$ kg, $m_3 = m_9 = 1621229$ kg,
$m_4 = 482290.5$ kg, $m_5 = 500952.74$ kg, $m_6 = 323769$ kg,

$K_{y1} = K_{y7} = 1.043 \times 10^{10}$ N/m, $K_{y2} = K_{y8} = 1.082 \times 10^{10}$ N/m, $K_{y3} = K_{y9} = 6.993 \times 10^9$ N/m,
$K_{y4} = 5.413 \times 10^7$ N/m, $K_{y5} = 1.53 \times 10^8$ N/m, $K_{y6} = 1.63 \times 10^8$ N/m,

$c_{y1} = c_{y7} = 5.2116 \times 10^7$ kg/s, $c_{y2} = c_{y8} = 5.4099 \times 10^7$ kg/s, $c_{y3} = c_{y9} = 3.4968 \times 10^7$ kg/s,
$c_{y4} = 1.0827 \times 10^6$ kg/s, $c_{y5} = 3.0598 \times 10^6$ kg/s, $c_{y6} = 3.2593 \times 10^6$ kg/s

$$F_{y1}^Y = F_{y2}^Y = F_{y3}^Y = F_{y7}^Y = F_{y8}^Y = F_{y9}^Y = 2.37 \times 10^7 \mathrm{N}$$

$$F_{y4}^Y = 9.28 \times 10^5 \mathrm{N};\; F_{y5}^Y = 9.28 \times 10^5 \mathrm{N};\; F_{y6}^Y = 9.28 \times 10^5 \mathrm{N}$$

For the non-linear viscoelastic pounding force model's parameters, the following values are assumed

$\beta = 2.6 \times 10^9$ N/m$^{3/2}$, $\xi = 0.25$ $(e = 0.73)$.

The initial separation gap between buildings is equal to $d = 0.02$ m. In order to accurately reproduce the actual pounding-involved response of the three bodies, the values of the parameters K_{yi} and F_{yi}^Y $(i = 1, \ldots, 9)$ have been verified comparing the MIDAS-Gen and MATLAB time-history analysis results in the hypothesis of elastic behaviour of the storey shear forces and assuming the same viscoelastic model for impact. Moreover the influence of torsional effects has been neglected.

The final results of the analysis in the hypothesis of elastic-perfectly plastic behaviour of the storey shear forces, obtained by "*main-pounding*" algorithm, are reported in Figs. 12-13. In particular Figs. 12 and 13 show the displacement and pounding force time-histories for the first, the second and third storeys of the left masonry and reinforced concrete bodies, respectively. The displacements and pounding forces of the right masonry body are similar to the ones of the left masonry body and therefore are not reported. The results indicate that the contact points at the level of the third storeys are the most critical ones for the pounding problem since collisions occur twenty times during the earthquake and pounding force reaches its maximum value. It is also evident that under the seismic action the response of the lighter and more flexible reinforced-concrete building is significant, while the displacements of the heavier and stiffer masonry bodies are nearly negligible.

Fig. 14 shows the shear force time-histories for the first, the second and third storeys of the left

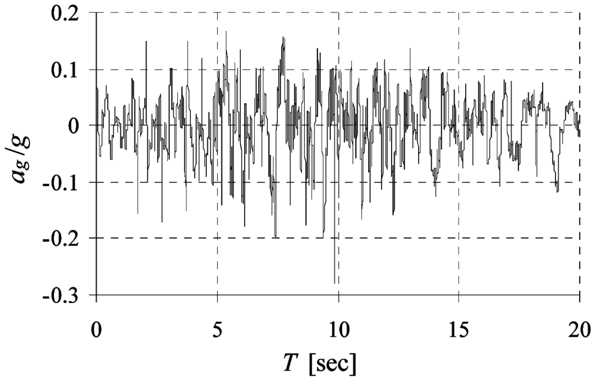

Fig. 11 Generated accelerogram of Bari

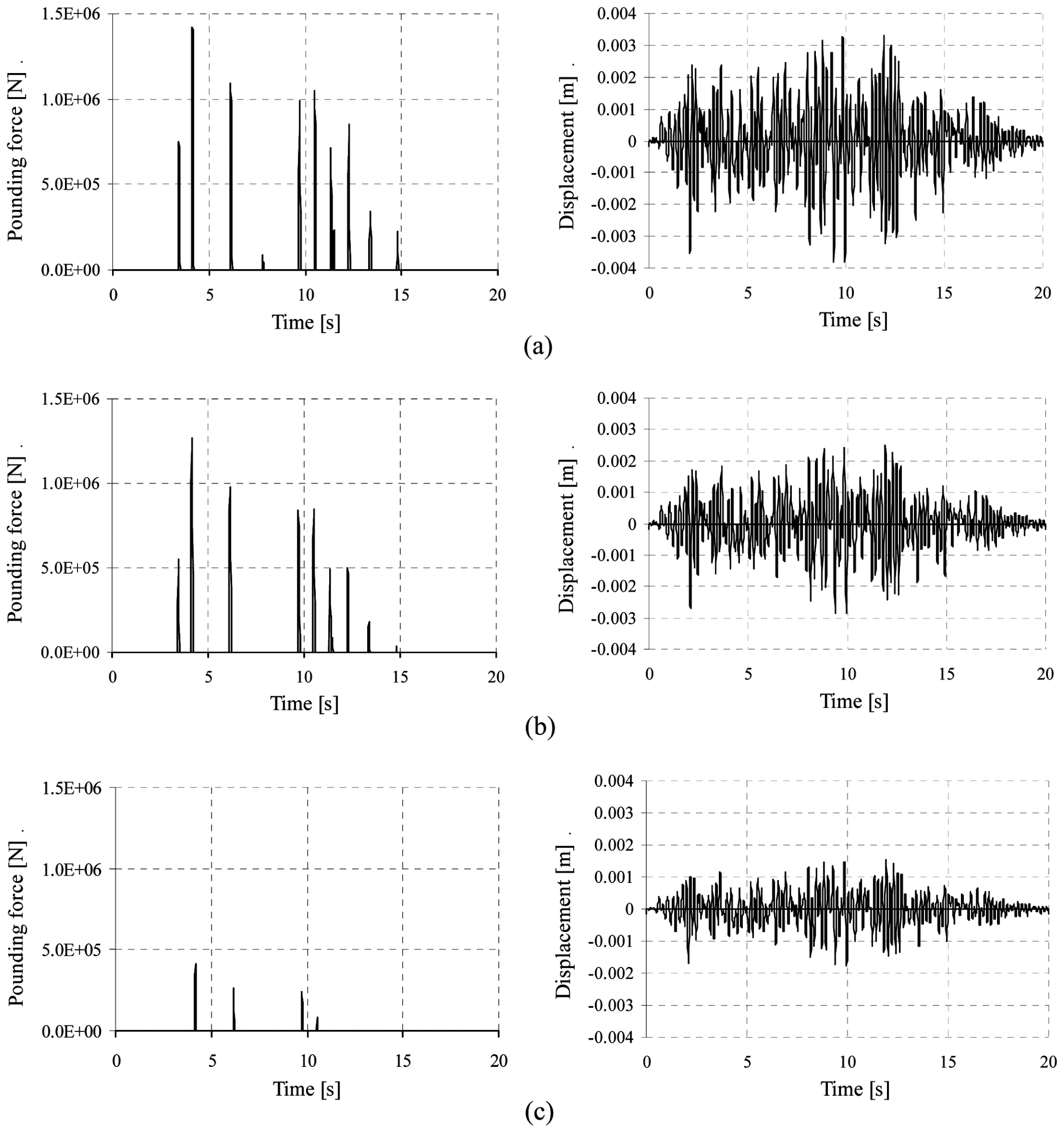

Fig. 12 Pounding force and displacement time histories of the left masonry body in the hypothesis of elastic-perfectly plastic behaviour of the storey shear forces: (a) node 3; (b) node 2; (c) node 1

masonry and reinforced concrete bodies. It is evident that only the first storey of the reinforced concrete building enters into the yielding range, resulting in a substantial permanent deformation of the structure.

Fig. 15 shows a comparison between the pounding-involved and independent vibration (large separation gap) responses of the left masonry body (node 3) and reinforced concrete building (node 6); also the shear force time-histories of the first, the second and third storeys of the reinforced concrete building can be compared with the values corresponding to the independent vibration case, reported in Figs. 16(a), (b) and (c). It emerges that the longitudinal response of the reinforced concrete building changes substantially as the result of collisions. The change in the structural

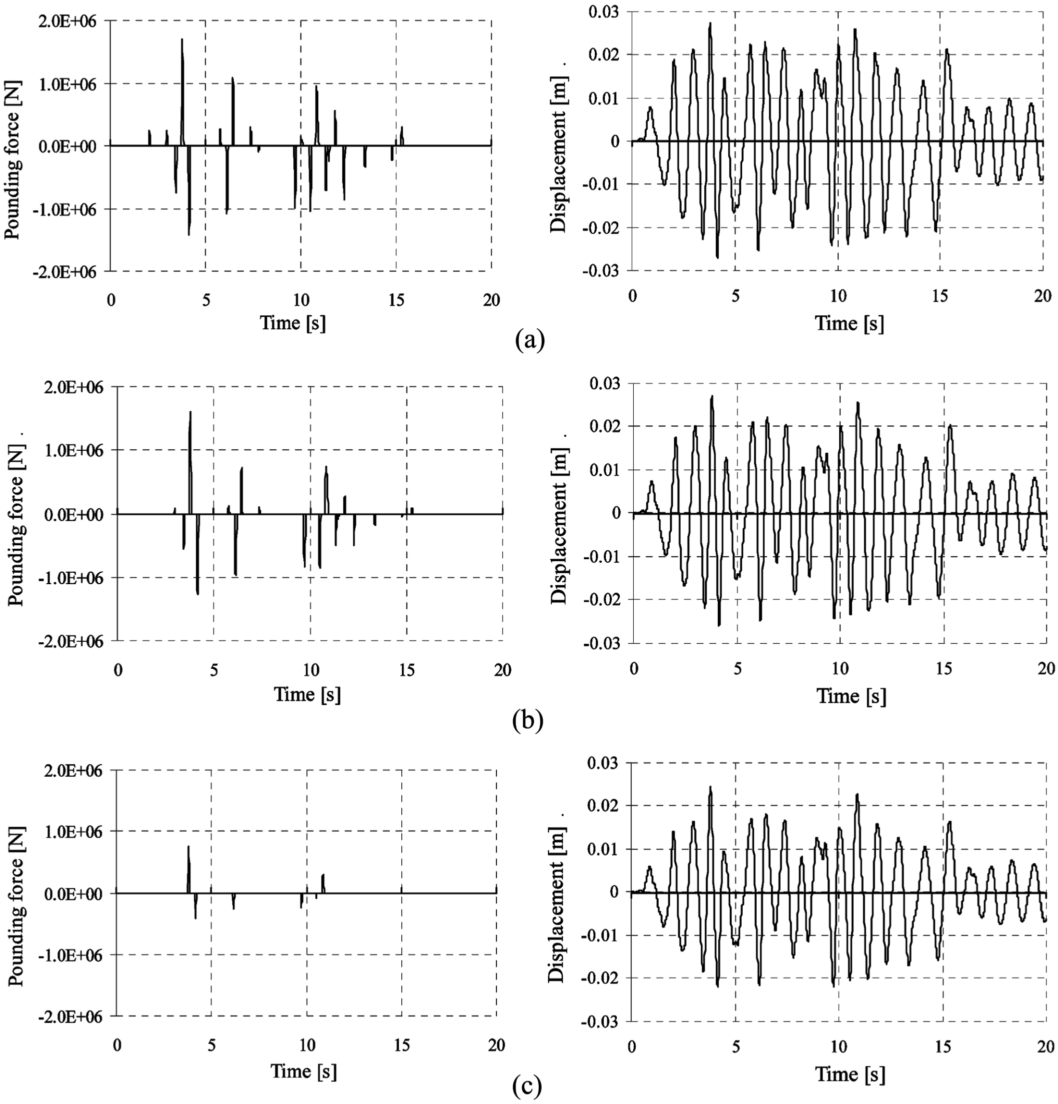

Fig. 13 Pounding force and displacement time histories of the reinforced concrete building in the hypothesis of elastic-perfectly plastic behaviour of the storey shear forces: (a) node 6, (b) node 5, (c) node 4

behaviour is due to friction forces, which develop at the time of collisions; these forces lead to a reduction of its overall response and to a phase shift, as it can be seen in Fig. 15(b). As a consequence the values of the peak displacements and of the storey shear forces of the pounding-involved response decrease with respect to the independent vibration case. The behaviour of the masonry building is contrarily nearly unaffected by collisions between structures.

Obviously the just described results derive by the particular position of the reinforced concrete building, situated between two bodies of the masonry one. In absence of one of the two masonry bodies the response of the reinforced concrete building would in fact increase due to structural pounding, as it can be seen from Figs. 16(d), (e), (f) and 17, where only the left masonry body is considered. In particular in this case both peak response and storey shear forces would increase if

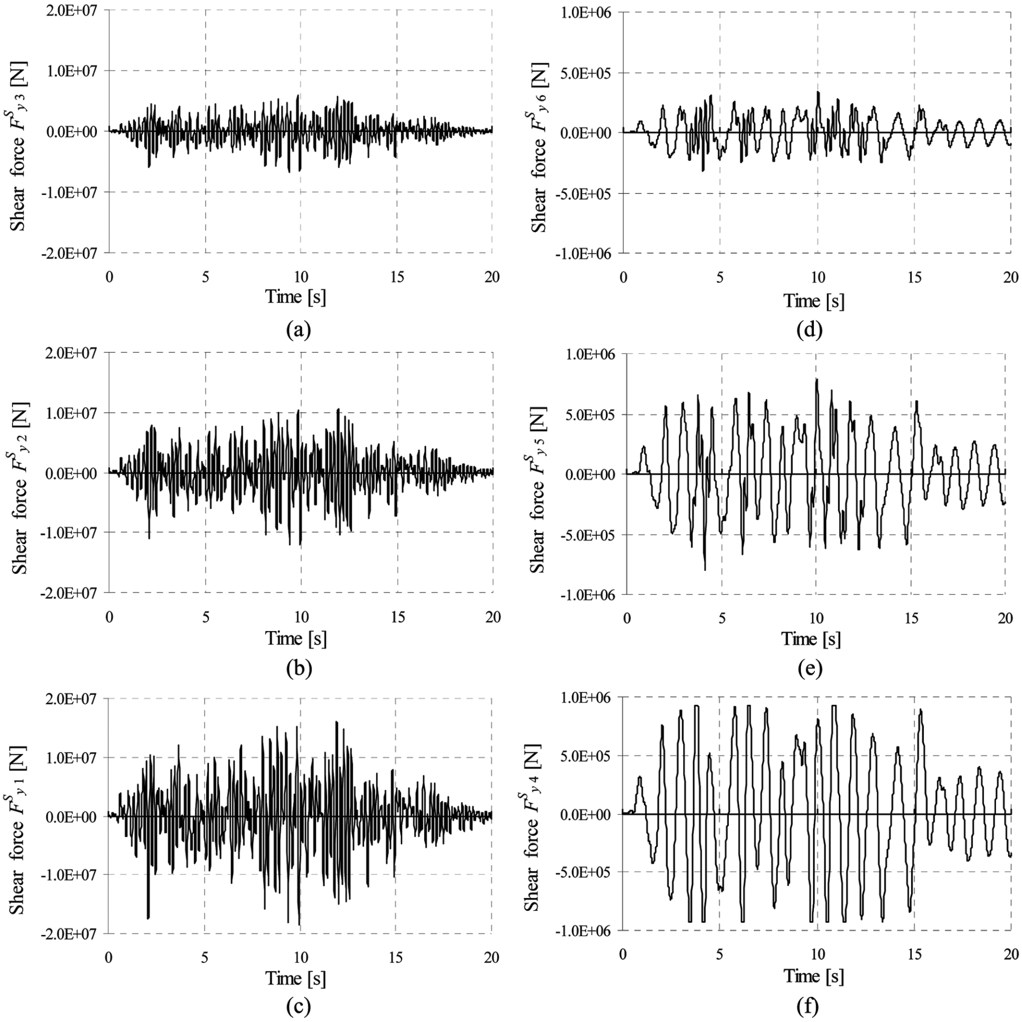

Fig. 14 Shear force time-histories of the left masonry body (a, b, c) and reinforced concrete building (d, e, f).

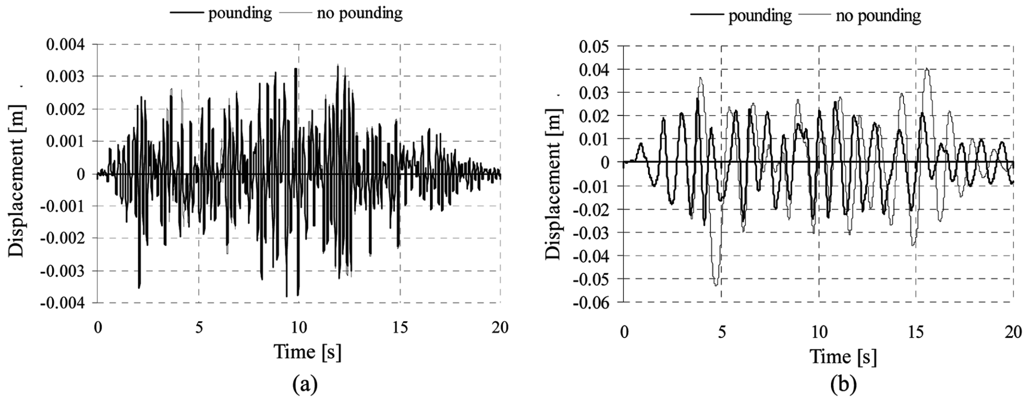

Fig. 15 Comparison between pounding response and independent vibrations of node 3 of the left masonry body (a) and node 6 of the reinforced concrete building (b)

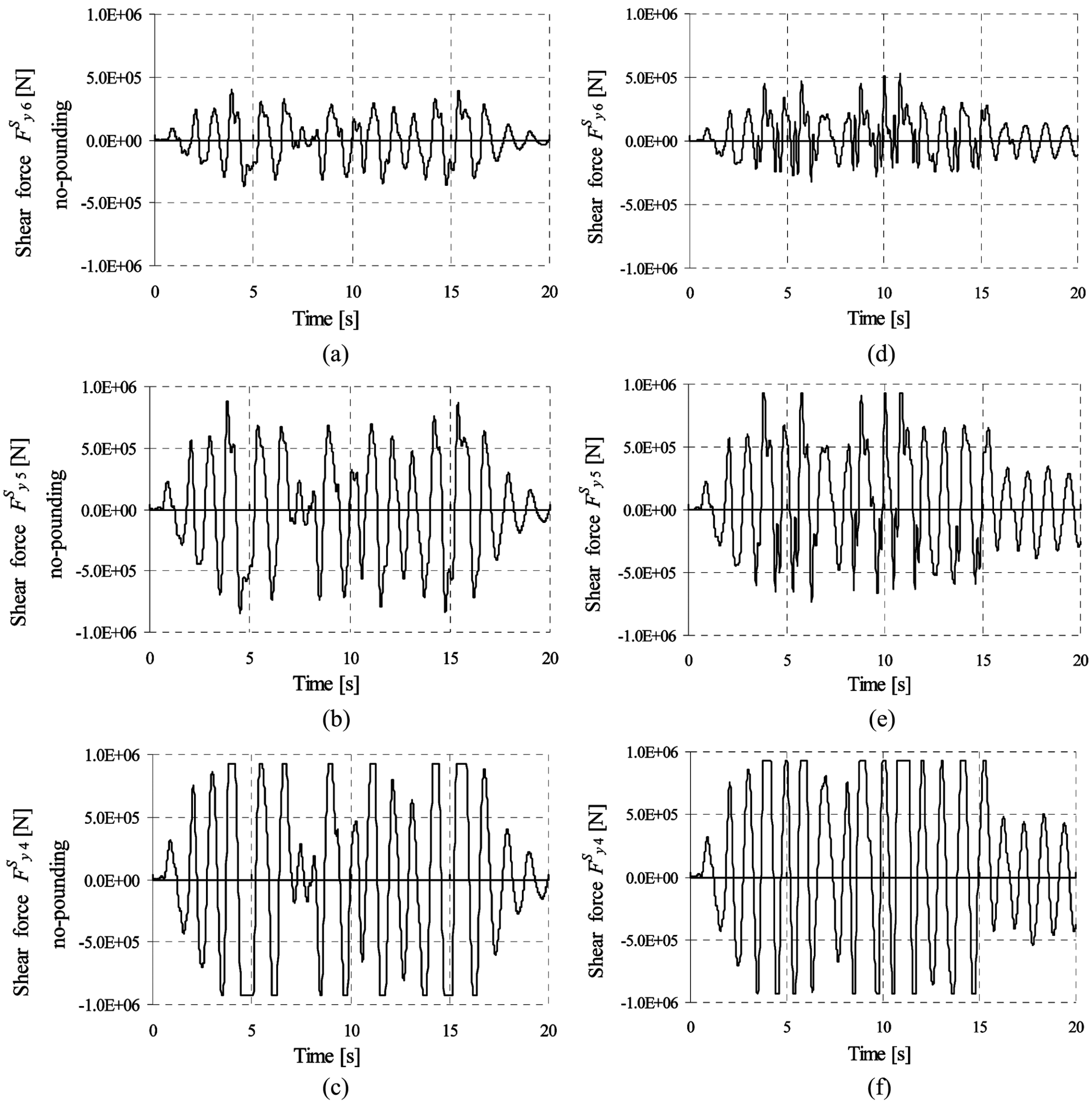

Fig. 16 (a), (b), (c) Shear force time-histories of the reinforced concrete building in the case of independent vibrations, (d), (e), (f) shear force time-histories of the reinforced concrete building in the hypothesis of just two buildings

compared to the independent vibration case.

Moreover it is worth noticing that the coefficient of restitution e, accounting for the energy dissipation during impact, depends on the actual material properties of the colliding structures and on the specific contact surface geometry (Jankowski 2005). Typical values for the coefficient of restitution in the case of real collisions between structures are about 0.5-0.75, especially referring to concrete structures and steel or concrete bridges (Anagnostopoulos and Spiliopoulos 1992). So, even if experimental data about impacts between concrete and masonry elements are not available in literature, the value of e used in this numerical application and set according to Eq. (13) is consistent with the literature values just mentioned.

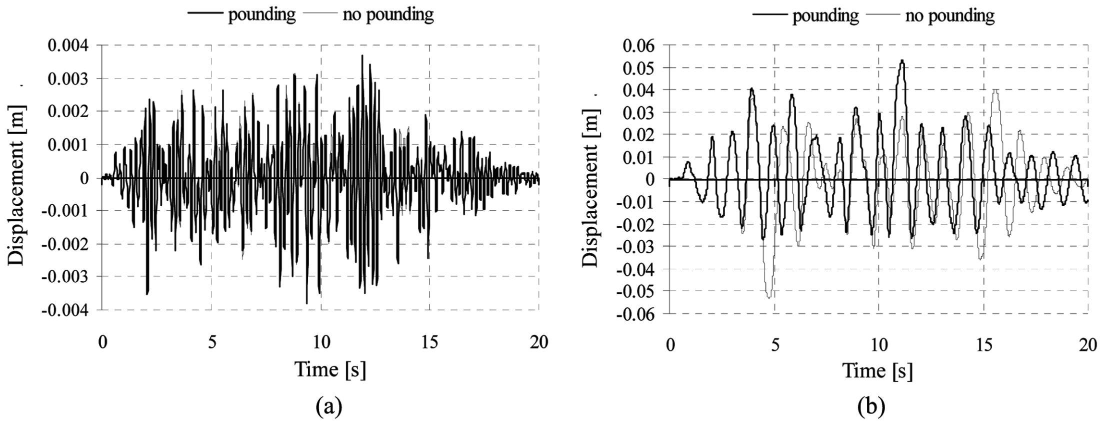

Fig. 17 Comparison between pounding response and independent vibrations of node 3 of the left masonry body (a) and node 6 of the reinforced concrete building (b) in the hypothesis of just two buildings

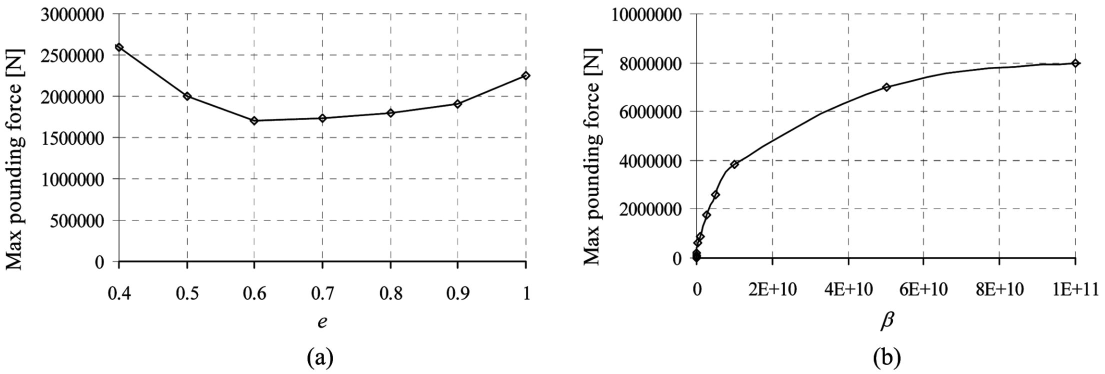

Fig. 18 Variation of the maximum pounding force at node 6 with: (a) the coefficient of restitution e; (b) the stiffness parameter β

However other studies indicate that collisions between structural members can be more plastic in some cases (Zhu *et al.* 2002). So, in order to provide additional information about this aspect, Fig. 18(a) shows how the value of the maximum pounding force at node 6 varies with the coefficient e. It emerges that reducing the energy dissipation due to impact ($e \rightarrow 1$) implies the overestimation of the earthquake-induced pounding effects with respect to the values herein obtained by adopting $e = 0.73$; more precisely in the interval $0.6 \leq e \leq 1$ there is an increment of the pounding force, while in the interval $0.4 \leq e \leq 0.6$ its value decreases. A detailed investigation of the value of e may thus lead to a more precise simulation of the structural pounding during earthquakes.

Finally also the impact stiffness parameter β is one of the key parameters of the model herein analyzed; in absence of experimental data validating the value used in the numerical application, Fig. 18(b) shows the variation of the maximum pounding force at node 6 with the coefficient β.

4. Conclusions

In the present paper a detailed pounding-involved response analysis of three adjacent structures has been carried out. The study has concerned pounding between two bodies of the "Quinto Orazio Flacco" school main masonry building and the reinforced concrete structure built in the long run along its free perimeter. The pounding risk has been outlined by the results of the pushover analyses of the involved buildings, conducted on suitable three-dimensional finite elements models of the whole structures.

In order to investigate the pounding-involved response, a suitable numerical procedure has been elaborated by MATLAB software. Both a non-linear viscoelastic model to simulate impact and a non-linear behaviour of the storey shear force have been employed in the algorithm, differently from many commercial softwares which admit just one non-linearity. This aspect makes the presented procedure particularly useful for practical purpose. Each colliding 3-storey building has been modelled as a three-degree-of-freedom system, with each storey's mass lumped on the floor level; in order to reproduce the actual behaviour of the buildings, the numerical algorithm has been calibrated on the basis of the three-dimensional finite elements model, comparing the results of the corresponding time-history analyses in the hypothesis of elastic behaviour of the storey shear force.

The proposed procedure represents a simple and effective method for properly simulating, with a small numerical burden, the seismic-pounding response between three colliding structures. With reference to the case study herein analyzed, the results show that collisions have a significant influence on the response of the lighter and more flexible reinforced-concrete building, while the behaviour of the heavier and stiffer masonry building is nearly unaffected by pounding. In fact, due to friction actions, the response of the reinforced concrete building changes substantially as the result of collisions, with a reduction of both peak displacements and storey shear forces with respect to the independent vibration case.

Finally it emerges the importance of an exact estimation of the coefficient of restitution and of the impact stiffness parameter in order to properly evaluate the pounding-involved effects.

References

Anagnostopoulos, S.A. and Spiliopoulos, K.V. (1992), "An investigation of earthquake induced pounding between adjacent buildings", *Earthq. Eng. Struct. Dyn.*, **21**, 289-302.

CEN (2001), "Eurocode 2. Design of concrete structures - Part 1: General rules and rules for buildings", EN 1992-1.

CEN (2003), "Eurocode 8. Design of structures for earthquake resistance - Part 1: general rules, seismic actions and rules for buildings ", UNI EN 1998-1:2003.

CEN (2005), "Eurocode 6. Design of masonry structures. Part 1-1: General rules for reinforced and unreinforced masonry structures", UNI EN 1996-1-1:2006.

FEMA (2000), "FEMA 356. Prestandard and commentary for the seismic rehabilitation of buildings", Federal Emergency Management Agency, Washington, D.C., USA.

Jankowski, R. (2005), "Non-linear viscoelastic modelling of earthquake induced structural pounding", *Earthq. Eng. Struct. Dyn.*, **34**(6), 595-611.

Jankowski, R. (2006), "Analytical expression between the impact damping ratio and the coefficient of restitution in the non-linear viscoelastic model of structural pounding", *Earthq. Eng. Struct. Dyn.*, **35**(4), 517-524.

Jankowski, R. (2008), "Earthquake-induced pounding between equal height buildings with substantially different dynamic properties", *Eng. Struct.*, **30**, 2818-2829.

Jankowski, R. (2009), "Non-linear FEM analysis of earthquake-induced pounding between the main building and the stairway tower of the Olive View Hospital", *Eng. Struct.*, **31**, 1851-1864.

M.I.T. (2008), *D.M. 14/01/2008. Norme Tecniche per le Costruzioni*, Ministero Infrastrutture e Trasporti, Rome, Italy.

Magenes, G. and Calvi, M. (1997), "In-plane seismic response of brick masonry walls", *Earthq. Eng. Struct. Dyn.*, **26**, 1091-1112.
Mistler, M., Butenweg, C. and Meskouris, K. (2006), "Modelling methods of historic masonry buildings under seismic excitation", *J. Seismol.*, **10**: 497-510.
Muthukumar, S. and DesRoches, R. (2006), "A Hertz contact model with non-linear damping for pounding simulation", *Earthq. Eng. Struct. Dyn.*, **35**: 811-828.
P.C.M. (2005), *Norme tecniche per il progetto, la valutazione e l'adeguamento sismico degli edifici,* Testo integrato dell'Allegato 2 - Edifici - all'Ordinanza 3274 come modificato dall'OPCM 3431 del 3/5/05, Italy.
Salonikios, T., Karakostas, C., Lekidis, V. and Anthoine, A. (2003), "Comparative inelastic pushover analysis of masonry frames", *Eng. Struct.*, **25**, 1515-1523.
Tomaževiĉ , M. (1999), *Earthquake resistant design of masonry buildings*, Imperial College Press, London.
Ye, K. and Li, L. (2009), "Impact analytical models for earthquake-induced pounding simulation", *Front. Archit. Civil Eng. China*, **3**(2), 142-147.
Zhu, P., Abe, M. and Fujino, Y. (2002), "Modelling three-dimensional non-linear seismic performance of elevated bridges with emphasis on pounding of girders", *Earthq. Eng. Struct. Dyn.*, **31**, 1891-1913.
Zou, X.K. and Chan, C.M. (2005), "Optimal seismic performance-based design of reinforced concrete buildings using nonlinear pushover analysis", *Eng. Struct.*, **27**, 1289-1302.

CC